Giovanni Cascante[1] *and Carlos Santamarina*[2]

Low Strain Measurements Using Random Noise Excitation

REFERENCE: Cascante, G. and Santamarina, C., **"Low Strain Measurements Using Random Noise Excitation,"** *Geotechnical Testing Journal*, GTJODJ, Vol. 20, No. 1, March 1997, pp. 29–39.

ABSTRACT: Low-strain wave propagation velocity and attenuation are effective measures of state in particulate media. The standard resonant column test procedure is modified to facilitate the study of wave propagation at low strains. The system uses band-limited random noise excitation in combination with signal averaging to control the signal-to-noise ratio. This procedure is efficiently implemented by replacing typical peripheral devices with a signal analyzer and computer control. The methodology permits testing at very low strains ($\gamma \approx 10^{-8}$). The effect of non-linear system response on computed transfer functions is addressed. Other results include the analytical treatment of coupling between torsional and transverse modes, the evaluation of local low-strain shear parameters from solid specimens tested in torsion, and the use of multi-mode testing for the evaluation of field parameters.

KEYWORDS: mechanical waves, resonant column, velocity, attenuation, random vibration, sands, transfer function, modal testing, non-linear behavior

Notation

- ϵ_z Axial strain
- γ Shear strain (γ^* reference shear strain at $G = G_{max}/2$, γ_R shear strain at $r = R$)
- γ_n Normalized shear strain = (γ_R/γ^*)
- $\gamma(\omega)$ Coherence function
- η, ι Exponents in the stress-damping relationship (isotropic stress)
- κ Wave angular number
- λ Wave length
- θ General angle
- σ_0 Isotropic confinement
- τ Shear stress
- ν Poisson's ratio
- ω Wave angular frequency (ω_n undamped natural circular frequency)
- d_{max} Maximum displacement
- e Void ratio
- h Constant given by $(h)^2 = (I_p/m_T L^2)$
- m_T Mass of the system (m added mass at the free end of the system)
- n Number of averages
- r Distance from the center of the specimen
- c Ratio of the mass of the sample to the mass of the driven plate
- cv Coefficient of variation = (standard deviation)/(mean)
- A Constant
- A_{max} Maximum acceleration
- C Constant
- C_c, C_u Coefficient of curvature and uniformity in grain-size distribution
- D Damping coefficient
- D_r Relative density
- DC Damping capacity
- D_{50} Diameter for 50% passing
- E Young's modulus
- $H(\omega)$ Transfer function
- I Mass polar moment of inertia of the specimen (z axis)
- I_b Area moment of inertia of the specimen (x axis)
- I_0 Mass polar moment of inertia of the driven plate (z axis)
- I_p Mass polar moment of inertia of the driven plate (x axis)
- J_p Area polar moment of inertia of the driven plate (z axis)
- J_s, J_r Area polar moment of inertia of the specimen and the rod
- $G_{ij}(\omega)$ Cross power spectral density of signals i and j
- G Shear modulus (G_{max} maximum shear modulus)
- G_s Unit weight
- L Length of the specimen
- R Radius of the specimen
- T Torque (T_0 torque for a constant shear modulus)
- V Wave velocity (V_s shear wave velocity)

Introduction

Low-strain wave propagation permits the study of geomaterial behavior and the monitoring of processes. The small perturbation involved in the measurement has little effect on the measurand. Wave propagation is characterized by frequency-dependent velocity and attenuation. The complementary evaluation of low-strain wave velocity and attenuation provides unique insight into the nature of various geo-processes, e.g., isotropic and anisotropic state of stresses, plastic deformations, cementation, contact failure, pore fluid changes, etc.

[1]Assistant professor, Civil Engineering Department, University of Waterloo, Waterloo, Canada.
[2]Associate professor, School of Civil and Environmental Engineering, Georgia Institute of Technology, Atlanta, GA (formerly at University of Waterloo, Waterloo, Canada).

Semi-empirical relationships between wave parameters and the state of stress are known. However, the effect of other variables is less well understood. Information is especially scarce on attenuation. In part, this is due to measurement difficulties, especially in the field: seismic velocities can be assessed with less than 10% error; however, one must expect large errors in attenuation measurements in part due to the uncertainty in geometric spreading and the presence of heterogeneities.

This paper documents the measurement procedure developed to study low-strain velocity and attenuation in particulate materials. The scope of the research includes varied contact behavior, surface properties, isotropic and anisotropic loading, and interpretation within the framework of micromechanical analyses (Cascante and Santamarina 1996; Santamarina and Cascante 1996). A brief review of experimental methods used to assess propagation parameters is presented first, followed by a discussion of the device and procedures developed for this research.

Laboratory Measurement of Velocity and Attenuation

There are three main laboratory methods used to determine the dynamic properties of soils at low strains: forced vibration, free vibration, and pulse propagation. Measurements can be conducted within different loading devices, including torsional shear, cubical shear, and axi-symmetric cells. Each method has its own limitations in attainable strain, load levels, and boundary conditions.

Resonant Column Testing by Forced Vibration

Resonant columns permit testing an axi-symmetric specimen under torsional and longitudinal excitation. There are different types of resonant columns depending on the boundary conditions and the mode of vibration. Wilson and Dietrich (1960) developed a fixed-free resonant column to measure both longitudinal and torsional vibrations. Hardin and Richart (1963) described two devices with free-free end conditions to measure torsional and longitudinal vibrations. Hardin and Music (1965) developed a resonant column device that allowed the application of deviatoric axial loads. All these devices were designed to operate at small strains (in the range of 10^{-5}). In 1967, Drnevich developed a free-fixed resonant column that allowed for strains greater than 10^{-4}. Later, devices that combine resonant column and torsional shear were designed to measure dynamic properties of soils for shear strains between 10^{-6} and 10^{-1} (Drnevich 1978; Drnevich et al. 1978; Isenhower 1980).

Two parameters are obtained from resonant column measurements: the resonant frequency and the material damping coefficient. Wave velocity and attenuation are computed from these measurements. The computation of the damping coefficient assumes an equivalent, uniform, linear viscoelastic specimen, i.e., Kelvin-Voigt model. This model predicts a response similar to the response observed in sand specimens even though damping in sands is not necessarily of a viscous nature (Hardin 1965; Hardin and Scott 1966; Roesset 1991). The frequency dependency of wave velocity and attenuation is difficult to obtain with this device because of problems involved in measuring high resonant modes (see Stoll 1979 for alternative approaches).

Several testing effects on resonant column results have been studied including: the effect of the number of cycles (Drnevich and Richart 1970), coupling between the specimen and the end platens (Drnevich 1978), restraint of the specimen due to end platens, and the stiffness of the membrane (Yu and Richart 1984; Drnevich (1985) suggested that the thickness of the latex membrane should be less than 1% of the specimen diameter). In general, these effects are negligible when the shear strain amplitude is small ($\gamma < 10^{-4}$). In addition, small deformations permit the assumption of in-plane strain conditions in data interpretation.

Decay of Free Vibration Testing

This method consists of measuring the free vibration response in a soil specimen once the system is released from an initial condition (displacement, velocity, or both). The single degree of freedom model is used to compute damping and resonant frequency; a model with multiple degrees of freedom could be used as well. Within a resonant column device, the initial velocity and displacement condition can be achieved by turning off the dynamic excitation produced by the driving mechanism. Data processing in this method is usually conducted in the time domain since the excitation occurs mainly in the first mode. However, higher vibration modes can be assessed in the frequency domain.

Pulse Propagation Testing

The two techniques discussed above provide information at a single frequency, which corresponds to the first mode of vibration. The study of wave propagation for different frequencies can be conducted by pulse propagation techniques, detecting the signal with two different receivers, or by detecting the signal and its reflection with the same receiver. The second alternative has the additional advantage that the transfer function of the soil-transducer coupling and peripheral systems can be analytically canceled. In either case, Fourier analysis of the first and second signals permits evaluating the frequency-dependent velocity and attenuation (Fratta and Santamarina 1996). Similar techniques are used to evaluate damping in situ; however, adequate corrections for geometric spreading are required in this case; this step makes field measurements quite uncertain (Ward and Toksöz 1971; Bourbie et al. 1987; EPRI 1993).

Resonant Column Testing: Assumptions and Modal Analysis

The closed-form solution for a cantilever beam with a rigid mass at its free-end presumes: continuum, linear elastic, isotropic, and homogeneous medium; one-dimensional wave propagation; no shear stresses acting on the wall of the specimen; radii remain straight during vibration; the driving system is rigid; and the specimen is fixed at the bottom. The validity of some of these assumptions in resonant column testing is assessed in the following paragraphs before close-form solutions for torsional and transverse modes are derived.

Strain Gradient

The shear strain varies radially throughout the specimen. Hollow-center specimens have been used to minimize strain gradient effects. However, due to the complexity in sample preparation, solid specimens are preferred. In this case, the selected representative value of strain is the shear strain at $r = 0.8 \cdot R$, where R is the radius of the specimen [ASTM Test Methods for Modulus and Damping of Soils by the Resonant-Column Method (D 4015)]. This is an average strain for the volume of the specimen.

The linear variation of strain in solid cylindrical specimens relates to a non-linear variation of the shear modulus, which is not compatible with the assumptions made in the dynamic solution of a solid specimen subjected to a torsional excitation. Consider a hyperbolic variation of the shear modulus G with shear strain γ,

$$G(\gamma) = \frac{G_{max}}{1 + \frac{\gamma}{\gamma^*}} \quad (1)$$

where G_{max} is the maximum shear modulus (low shear strain) and γ^* is a reference shear strain. A convenient choice of the reference strain in conjunction with the hyperbolic model is the strain at which the shear modulus is reduced $G_{max}/2$ (Ishihara 1986). Assuming static equilibrium, the torque T applied to a specimen of radius R is equal to the area integral of the shear stress τ:

$$T = \int_0^{2\pi R} \int_0 \tau r^2 \, dr \, d\theta \quad (2)$$

where r is the distance from the center of the specimen. The shear strain at distance r can be computed from the shear strain at the wall of the specimen γ_R, assuming a linear strain distribution, by $\gamma = \gamma_R[r/R]$, and $\tau = \gamma G(\gamma)$. Substituting into Eq 2, and normalizing with the torque T_0, for a section with constant shear modulus $G(\gamma) = G_{max}$, given by $T_0 = \pi G_{max} R^3 \gamma_R/2$,

$$\frac{T}{T_0} = 2(\gamma_n)^{-4}\left[2(\gamma_n) - (\gamma_n)^2 + \frac{2}{3}(\gamma_n)^3 - 2\ln(1 + \gamma_n)\right] \quad (3)$$

where the normalized shear strain γ_n is

$$\gamma_n = \frac{\gamma_R}{\gamma^*} \quad (4)$$

Equation 3 is plotted in Fig. 1. It is shown that the error on the computed value of G_{max} is less than 1% if the maximum strain at the wall of the specimen γ_R is less than 1% of the reference strain γ^*. Therefore, low strain measurements of stiffness can be performed accurately on solid specimens subjected to torsional excitation.

Straight Radii

Radii remain straight only for the first mode of a rod vibrating in torsional mode (Achenbach 1975). The specimen with the driving plate will vibrate in the first mode when the ratio between the mass polar moment of inertia of the specimen (I) to the mass polar moment of inertia of the driving system (I_0) tends to zero. Therefore, the influence of higher resonant modes will disappear.

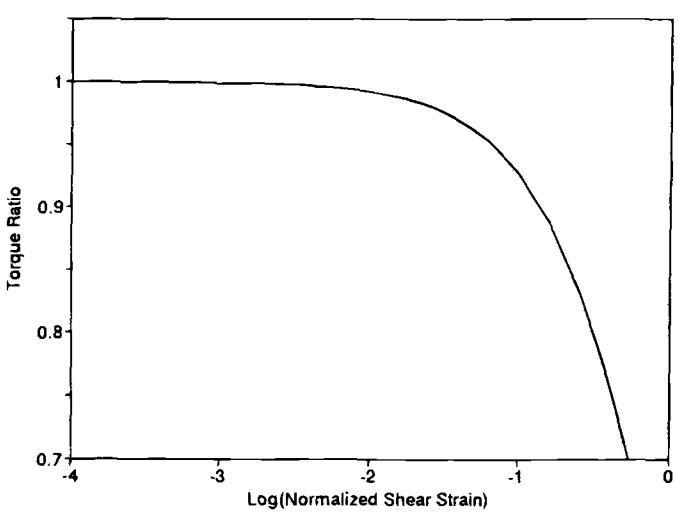

FIG. 1—*Effect of the strain-dependent shear modulus on cross-sectional torque. The reference strain γ^* corresponds to* $G = G_{max}/2$.

Lower Boundary

The impedance mismatch between the specimen and the resonant column pedestal can play an important role in the energy dissipation mechanism. If boundary conditions are ignored, the damping calculated could include both specimen and apparatus damping. On the other hand, if the relative stiffness of the apparatus with respect to the specimen is not enough to ensure the fixed condition, the shear modulus will be underestimated. Drnevich (1978) recommended that the stiffness of the fixed end of the resonant column should be at least ten times the stiffness of the specimen. Avramidis and Saxena (1990) stiffened a Drnevich-type resonant column in order to test specimens with resonance frequencies greater than 300 Hz, which was the upper bound of the original apparatus. They found important differences between the results of the original apparatus and the modified one for a Monterey sand No. 0 subjected to 588 kPa of confinement. The effect was more pronounced on the measured damping coefficient. Ashmawy and Drnevich (1994) recommended the use of a three-degree-of-freedom model to account for not perfectly fixed boundary conditions, particularly when the natural frequency of the soil-apparatus system is close to that of the passive end or reaction system in a Drnevich-type resonant column.

The effect of bolting the resonant column device to a high-mass base was found to be negligible for low strain tests conducted in this study, $\gamma < 10^{-5}$ where the resonant column was modeled as a fixed-free system. The fixed-free condition was confirmed by placing an accelerometer at the base of the resonant column device. Bolting it is important for large strains, especially for damping measurements.

For stiff specimens, the spring model (one spring at the base) is more appropriate. Both configurations have a node at the base for the first resonant mode (Hardin 1965); thus, either model gives an accurate representation of the real system. The response of the spring model depends on the properties of the base; however, the ratio of responses measured at the top and at the bottom is independent of those properties (Hardin 1965).

Dynamic Analysis—Mode Coupling

Most resonant column devices include a rigid mass at the top of the soil specimen. The effect of this mass is important for the calculation of shear wave velocity and the shear strain at resonance. As the rigid mass tends to zero, the first torsional mode approaches a quarter sine wave; hence, the shear strain is not constant throughout the height of the specimen. As the rigid mass tends to infinity compared with the mass of the specimen, the first mode approximates a straight line and the shear strain is constant at a given radius (Woods 1978).

The governing equation of motion for the fixed-free torsional resonant column is (e.g., Richart, Hall, and Woods 1970):

$$\frac{1}{\kappa L} = \frac{I_0}{I}\tan(\kappa L) \quad (5)$$

where the wave number is $\kappa = \omega_n/V_s$, ω_n is the undamped natural circular frequency, L is the length of the specimen, and V_s is

the shear wave velocity. The damped resonant frequency (ω_r) is measured instead of ω_n. However, $\omega_r \approx \omega_n$ for small values of the material damping coefficient ($D < 20\%$).

Equation 5 applies only when torsional modes are excited; therefore, the longitudinal axis of the specimen must be perpendicular to the pedestal, and the top platen must be perfectly horizontal. In practice, deviations take place and transverse motion develops. Comparing transverse and torsional resonant frequencies permits establishing the influence of transverse modes on the response. The free vibration equation of motion for a cantilever beam with a rigid mass at the free end was solved to compute resonant frequencies of transverse modes. The transcendental equation for transverse modes in terms of the ratio of the mass of the specimen to the mass of the driving plate ($c = m_T/m$) and the wave number κ is (Cascante 1996):

$$\sin(\kappa L) = \frac{\cos(\kappa L)}{\left(\frac{c}{\kappa L} - 2h^2 c\kappa L\right)}\left[\left(\frac{c^2}{(\kappa L)^2} + (h\kappa L)^2\right) + \frac{\left(\frac{c^2}{(\kappa L)^2} - (h\kappa L)^2\right)}{\cos(\kappa L)\cosh(\kappa L)} + \tanh(\kappa L)\left(\frac{c}{\kappa L} + h^2 c\kappa L\right)\right] \quad (6)$$

where h is a coefficient that relates the mass polar moment of inertia of the driving plate I_p (axis perpendicular to the axis of the specimen), with the mass of the specimen m_T by $I_p = (Lh)^2 m_T$. Once κL is known, the natural frequency of the transverse mode is computed as $(\omega_f)^2 = EJ_b(\kappa L)^4/(m_T L^3)$, where E is the Young's modulus, and J_b is the area moment of inertia of the specimen.

Equations 5 and 6 permit the analysis of mode coupling. The solution for κL is obtained numerically. Alternatively, the left and right sides of these equations can be plotted to identify the points of intersection, as shown in Fig. 2: the first intersection of the solid lines with the dashed lines represents the solution for the first torsional and flexural modes (Figs. 2*a* and 2*b*, respectively).

Approximate solutions for flexural and torsional resonant frequencies using Rayleigh's method are:

$$\omega_f^2 = \frac{6EI_b}{L^3\left[\frac{33}{70}m_T + 2m + 6m\frac{l_0}{L} + \frac{9}{2}m\left(\frac{l_0}{L}\right)^2\right]} \quad (7)$$

$$\omega_T^2 = \frac{GJ_p}{L\left[\frac{I}{3} + I_0\right]} \quad (8)$$

where J_p is the area polar moment of the specimen and l_0 is the distance between the top of the specimen and the centroid of the top mass. Mode coupling becomes more important when the mass of the driving system increases with respect to the mass of the specimen.

Resonant Column Testing with Random Noise Excitation

The standard test method for the resonant column device is based on harmonic excitation sweeping the frequency around resonance. The response curve is determined with small frequency increments in order to get precise values of damping and resonant frequency. This procedure is time consuming, especially for low damping because many points are needed to define the sharp resonant peak. Moreover, for very low strain measurements the system response in the time domain is strongly affected by background noise. Improvements can be obtained by processing in the frequency domain, either by obtaining long-time records or by averaging short ones.

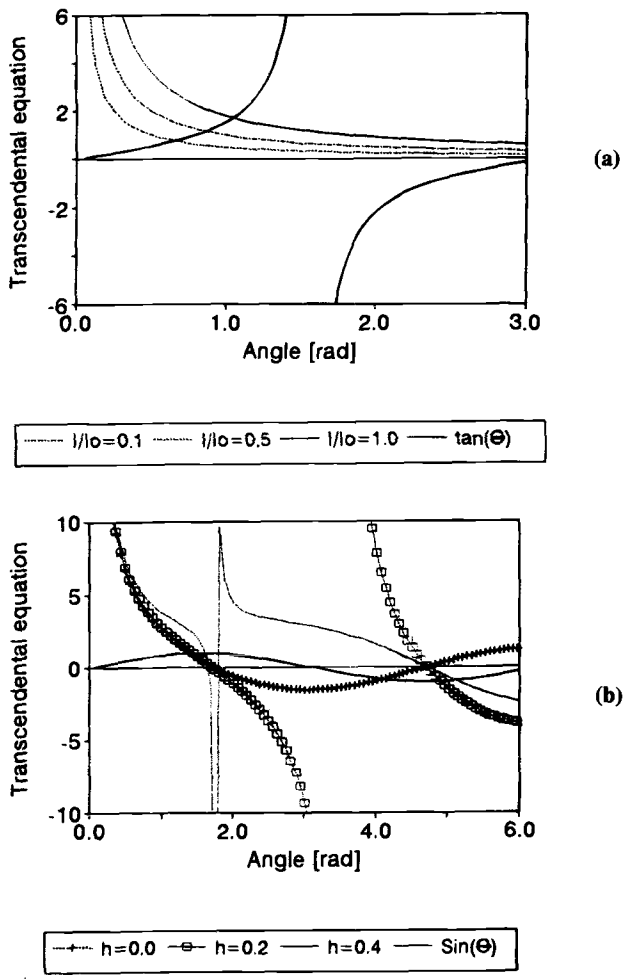

FIG. 2—*Plot of left and right sides of transcendental equations, where the angle* $\theta = \kappa L$: (a) *torsional modes for different ratios* I/I_0; (b) *flexural modes for different values of* $h = (I_p/m_T L^2)^{0.50}$.

The standard test procedure was modified to excite the specimen with random noise (Prange 1981; Aggour et al. 1988; Amini et al. 1988). Random noise imposes all frequencies simultaneously, spreading the energy in the selected frequency band, facilitating low-strain measurements, $\gamma < 10^{-6}$.

Device

A Stokoe torsional-resonant column device was used in this research (SBEL D1128). The cell and specimen pressures are independently controlled by a Brainard-Kilman pneumatic pressure control panel, which allows confining pressures up to 700 kPa to be applied. The axial deformation of the specimen is measured with a LVDT (Schaevitz 500HR) mounted inside the confining chamber. The input signal for the driving coils is generated by a function/arbitrary waveform generator (HP-33120A or the built-in signal generator in a dynamic signal analyzer HP-35665A) through a power amplifier (Krohn-Hite 7500). During resonant

testing, the response of the specimen to torsional vibrations is monitored with one accelerometer mounted at the top and one on the base (Columbia Research 8402 and charge amplifier 1035). The output signal from these transducers is monitored and processed in a digital storage oscilloscope (HP-54600A with a HP-54657A Module), a universal counter (HP-53131A), a dynamic signal analyzer (HP-35665A), and by software developed as part of this research, running in a PC 486. Figure 3 presents a schematic view of the device. The instruments shown in the figure are the minimum components recommended to run the test with random noise excitation.

The driving system is 15 cm in diameter, which is close to the height of the specimen. The solution neglecting the inertia of the driving system in the transverse direction is a good approximation just for the first mode of vibration, even in the extreme case when the radius of gyration is computed assuming the mass of the driving system concentrated at the position of the four magnets (h = 0.4; Fig. 2*b*). For this device with $c = m_T/m$ smaller than 4, approximate Eqs 7 and 8 have less than 0.3% error with respect to the theoretical values obtained with Eqs 5 and 6. For typical soils, levels of confinement (10 to 700 kPa), and standard specimen size (H = 13 cm, R = 3.5 cm), the torsional frequency is about 60% higher than the flexural frequency ($\omega_T \approx 1.6\omega_f$). Thus, mode coupling can be neglected.

Calibration—Driving System

The computation of the shear wave velocity in the resonant column test requires the mass polar moment of inertia of the driving system I_0. In general, due to the complex geometry of driving systems, the experimental determination of I_0 is preferred. A metal calibration specimen and a mass are used to measure I_0 assuming a single degree of freedom system with total mass equal to the mass of the driving system plus any additional mass attached to the system. Several aluminum and steel probes were manufactured to verify calibration in different frequency ranges. Characteristics of the calibration probes are summarized in Table 1. Calibration probes were fastened to top and bottom platens with steel screws. Equipment modes in the range of frequency of interest were assessed with a solid steel specimen. No spurious modes were detected.

The mass polar moment of inertia of the driving system must be re-calibrated whenever changes are made, e.g., transducers added to the top cap. Errors in the measurement of frequency have a significant effect in the computation of I_0; for example, a 5% error in frequency can produce a 50% error in the computed inertia of the driving system.

Test Automation—Random Noise Excitation

The resonant column is computer controlled. The inter-communication between the computer and external devices is performed through an HP-IB interface card, which can drive a maximum of 14 devices simultaneously. Each device has a specific address, which is used in the software to send and to receive data from peripheral devices. The external devices that were selected permit control and programming with the Standard Commands for Programmable Instruments (SCPI). This language, together with the HP-IB interface card, allows remote control of instruments including: set up, measurement, and data transfer. Accelerometer signals are monitored mainly with the spectrum analyzer because of the flexibility and precision of this instrument.

The program initializes all devices. Then, it runs a broad-band random noise (400 Hz bandwidth) to identify the maximum peak in the frequency response curve, which corresponds to the first torsional resonant mode ω_r. Once the peak is selected, a 50-Hz bandwidth random noise centered around ω_r is used to compute the transfer function, input and output power spectral densities, and the coherence function. These curves are computed by averaging multiple measurements. The resonant frequency and the damping coefficient are computed in real time by the spectrum analyzer, curve fitting the frequency response within a 25-Hz bandwidth. When the frequency response curve near resonance is not single-

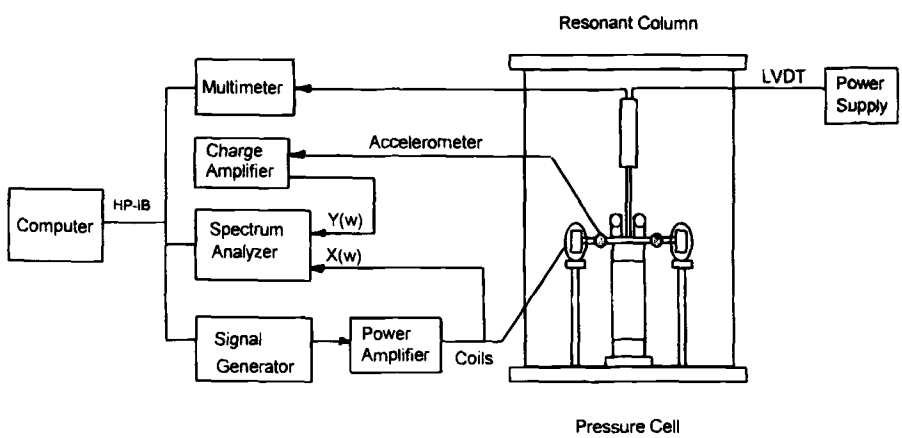

FIG. 3—*Resonant column and recommended devices for random noise excitation.*

TABLE 1—*Characteristic of calibration specimens.*

Material	Unit Weight, g/cm^3	Weight, g	Diameter Out, cm	Diameter In, cm	Length, cm	Resonant Frequency, Hz	Damping, $\times 10^3$
Steel	7.83	52.4	0.634	0.446	20.45	20.28	35.3
Aluminum	2.77	42.23	0.796	0.528	20.45	19.41	35.6
Aluminum	2.77	258.42	2.540	2.354	13.94	122.4	6.1
Aluminum	2.77	345.84	2.540	1.900	13.98	192.8	4.1

peaked, properties are checked during post-processing by curve fitting a multi-degree-of-freedom solution. Details of the test implementation and the computer code can be found in Cascante (1996).

Random Noise Excitation: Signal Processing

Test implementation with random noise excitation requires frequency domain signal processing techniques. In addition, two questions emerge in the implementation of this methodology: first, what is the accuracy of measurements in the presence of low signal-to-noise ratios? And, second, how can the characteristic strain level for the test be determined? These issues are addressed below.

Signal Processing

The input is the *voltage* $V_{in}(t)$ *at the coils*, and the output is the voltage delivered by the accelerometers $V_{out}(t)$, as shown in Fig. 3. The choice of monitoring location is relevant to avoid unmeasured signal components; for example, the back electromotive force generated at coils (EPRI 1993, Appendices for Laboratory Investigation) which would be an unmeasured input, yet correlated with the measured input.

The processing of results from random noise excitation assumes linear, time-invariance. The power spectral density of the input G_{xx} is linearly related to the cross power spectral density of the output and the input G_{yx} by the transfer function of the system $H(\omega)$:

$$H(\omega) = \frac{G_{yx}(\omega)}{G_{xx}(\omega)} \tag{9}$$

If the input is a pseudo-random noise, its auto-power spectral density is constant $|G_{xx}| = A_0$. Then, the cross-power spectral density G_{yx} is equal to the transfer function $H(\omega)$ scaled by A_0 (for the devices used in this study, the average amplitude of the PSD of the input random noise signal was linearly related to the voltage at the source). Alternatively, if the quasi-random input and the output signals are known, the transfer function can be computed from Eq 9. The transfer function is computed for the n input-output signals of period T using the average values G_{yx} and G_{xx} (averaging cancels the effect of output noise).

The coherence function γ^2 characterizes the level to which the output is linearly caused by the input, and it is mathematically defined as:

$$\gamma(\omega)^2 = \frac{\overline{G_{yx}G_{yx}^*}}{\overline{G_{xx}G_{yy}}} \tag{10}$$

where subscripts x and y refer to input and output signals; * denotes complex conjugate, and the bar over functions means average for multiple signals. When the coherence is $\gamma^2(\omega) = 1.0$, there is no noise, therefore all the output follows from the input, and the system behaves linearly. Coherence $\gamma^2(\omega) < 1.0$ may indicate input noise, an unmeasured input that is correlated with the measured input, or non-linearity. A sudden drop in coherence at the peak of $H(\omega)$ may also be due to deficient frequency resolution (Bendat and Piersol 1993). Coherence is related to the signal-to-noise ratio SNR:

$$\text{SNR}(\omega) = \frac{\gamma(\omega)^2}{1 - \gamma(\omega)^2} \tag{11}$$

Typical plots of coherence, power spectral density, and computed transfer functions from measurements in the resonant column are presented in Fig. 4. The plot of the coherence function confirms the linearity of the system required for the computation of $H(\omega)$. The dip at resonance $\gamma^2(\omega) = 0.96$ indicates resolution bias, while the dip at 120 Hz is due to electrical noise (Fig. 4*c*).

The smooth transfer function presented in Fig. 4*b* shows the beneficial effects of averaging. The evaluation of system parameters from $H(\omega)$ can be made with various transfer function estimators such as amplification at resonance, amplitude at two frequencies, or from the phase curve. Results may vary depending on the frequency resolution. In this study, the frequency resolution was 0.125 Hz (400 data points), and resonant frequency and damping were computed by least-square fitting a single degree of freedom model to the measured data set.

Noise and Error

The determination of smooth transfer functions and the computation of accurate dynamic parameters requires a significant amount of information in the presence of noise. Either long records (memory restrictions) or averaging is required. If the noise is Gaussian with zero mean, the standard deviation of the mean is reduced proportionally to $(n)^{1/2}$, where n is the number of averages. Then, the number of signals to be averaged (n) depends on the coefficient of variation (cv) of the amplitude of the transfer function at frequency f (cv = standard deviation/mean), and the coherence $\gamma^2(\omega)$ between input and output at that frequency (see related concepts in Bendat and Piersol 1993). For a single-point estimator (e.g., peak response), the number of averages required is:

$$n \approx \frac{1}{2cv^2}\left(\frac{1}{\gamma(\omega)^2} - 1\right) \tag{12}$$

For example, the number of signals n required to determine the value of the gain $|H(f)|$ with a $cv = 2\%$, when the coherence between input and output is $\gamma^2(\omega) = 0.8$, is $n = 312$. The error in $|H(f)|$ directly affects the computation of D in single-value computations; however, compensation takes place in least-square curve fitting the data with a single-degree-of-freedom model.

Characteristic Strain Level

Measurements are associated with a representative strain level corresponding to the measured response. When harmonic excitation is used in the frequency sweep method, the maximum strain at resonance is selected to characterize the effect of strain level on the measured dynamic properties. The maximum induced shear strain is computed from the maximum displacement d_{max} obtained from the accelerometer response:

$$d_{max} = A_{max}/\omega_n^2 \tag{13}$$

where A_{max} is the maximum acceleration at the resonant frequency ω_n. Equation 13 is exact for sinusoidal excitation (Sin-E), but it is an approximation for random excitation (Rnd-E). Amini et al. (1988) used the peak-shear strain of the response, estimated by analytically scaling the root-mean-square (RMS) shear strain. Al-Sandad et al. (1983) found that the *RMS of the measured displacement* yielded good agreement with results obtained using the RMS of sinusoidal excitation for damping and velocity.

The time response to band-limited random noise excitation resembles a sinusoidal response. Hence, the *RMS of the accelerom-*

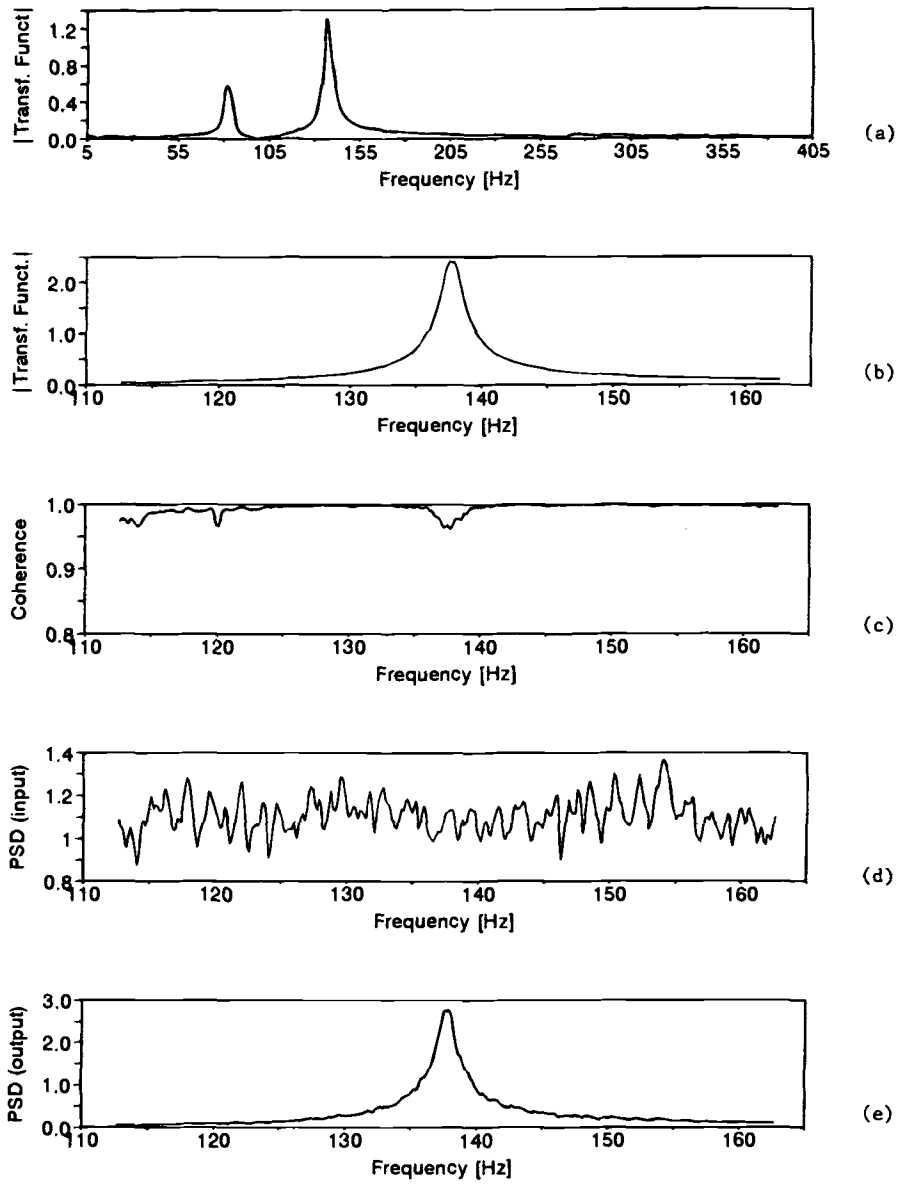

FIG. 4—*Typical resonant column data—random noise excitation:* (a) *broad-band transfer function,* (b) *narrow-band transfer function,* (c) *coherence function,* (d) *input power spectral density, and* (e) *output power spectral density.*

eter response was selected to estimate the maximum strain in this study. The RMS acceleration is calculated from the area under the output power spectral density within the frequency range used for random noise generation, from ω_1 to ω_2. Equation 13 becomes:

$$d_{\max} = \frac{\sqrt{2}\left[\int_{\omega_1}^{\omega^2} G_{yy}(\omega)\right]^{1/2}}{\omega_n^2} \qquad (14)$$

Sinusoidal and Random Excitation

A uniform, silica sand was tested in this study (Barco sand 32, D_{50} = 0.44 mm, $e_{\max}$ = 0.73, $e_{\min}$ = 0.49, C_u = 1.5, C_c = 0.96, SiO_2 content 99.6%, and G_s = 2.65). The specimen was prepared by the dry pluviation technique from a constant falling height ($e \approx 0.60$, $Dr \approx 54\%$; specimen length L = 0.13 m, diameter d = 7.1 cm). Once the upper platen was set in place, vacuum was applied to hold the specimen and the split mold was removed. Then, connections for the driving plate, LVDT, and accelerometer were made, and the chamber was assembled. Specimen vacuum was gradually released while increasing the cell pressure until an effective confinement σ_0 = 35 kPa was reached. Isotropic confining was increased from 35 to 200 kPa. This and other specimens were tested within 24 h after preparation. Measurements were performed 30 min after each load stage was applied, when emissions ceased.

The low-strain frequency response with random Rnd-E excitation and with the standard sinusoidal Sin-E excitation (constant input voltage) are presented in Fig. 5. This test was conducted at an effective confinement of σ_0 = 200 kPa. Low strain levels were achieved both in Rnd-E and Sin-E using the frequency domain capabilities of the signal analyzer (the signal-to-noise ratio was too low to use the standard oscilloscope-based procedure). A small frequency interval was used: Δf = 0.1 Hz for a bandwidth of 4 Hz around resonance, and Δf = 0.2 Hz away from resonance, for a total of 70 measurements. Results in Fig. 5 show that when the

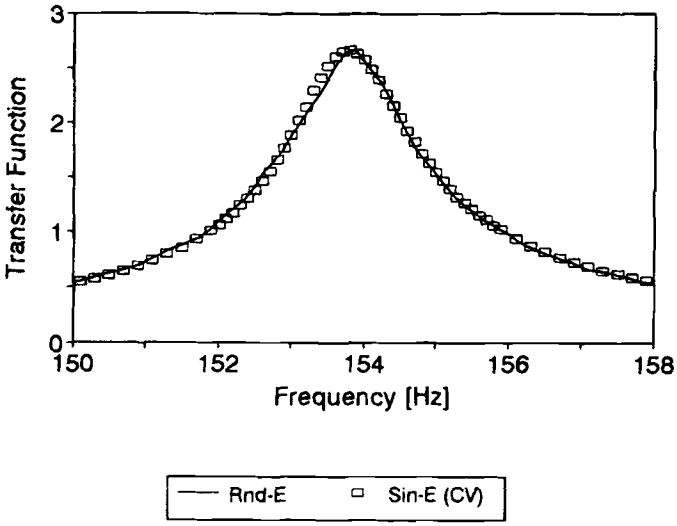

FIG. 5—*Comparison of transfer functions obtained at low strain ($\gamma = 10^{-5.6}$), with sinusoidal excitation at constant input voltage Sin-E(CV) and with random excitation Rnd-E.*

system behaves linearly, results from Rnd-E and the standard Sin-E are the same.

Non-Lineal Behavior and Random Noise Excitation

The test procedure with random noise excitation requires Fourier analysis, which presumes linear, time-invariant behavior. Therefore, it is appropriate for low strain testing. As the strain level increases, several difficulties develop. Results from an experimental study are presented next.

Once again, the specimen was confined to a constant effective stress σ_0 = 200 kPa, and the frequency response was determined using sinusoidal Sin-E and random Rnd-E excitations. The test was conducted sequentially, testing with Rnd-E and Sin-E at increasingly higher levels of strain in order to minimize the effects of specimen perturbation. After the maximum shear strain was reached ($\gamma = 10^{-4}$), the transfer function for low strain ($\gamma = 10^{-6}$) was measured again and compared with the initial value, showing minimum stress-history effects.

Figure 6*a* presents the evolution of the transfer function with increasing peak shear strain. Data points are shown only for two tests to highlight the data density; other data are plotted as lines. These curves are typical for non-linear systems (see a similar plot numerically obtained by Bolton and Wilson, 1990, with linear springs and frictional sliders). The system manifests a non-symmetric transfer function for strains $\gamma > \approx 2.5 * 10^{-5}$. The frequency response of the non-linear system varies rapidly just below resonance, and the test must be conducted with high-frequency resolution to clearly identify the non-linear response. The determination of D in this case can be in serious error. One alternative is to evaluate the decay of free vibration (EPRI 1993).

Selected frequency response curves using Rnd-E at different strain levels are shown in Fig. 6*b*. Curves shift to the lower frequencies with the increase in shear strain as for Sin-E. However, transfer functions remain symmetric, and each curve is accurately matched by a linear single-degree-of-freedom system, i.e., the system response appears "linearized."

Let us assess this result further. If the cause of non-linearity is amplitude dependent, then a sine-sweep test keeping the strain level constant would render the response of a "linearized" system for that strain level (Ewins 1984). This was verified by running sinusoidal excitation tests at constant strain Sin-E(CS); the shear strain was kept constant by adjusting the voltage of the input signal at each frequency to compensate the change in strain. Results for the three types of excitation are presented in Fig. 7*a*. There is a clear correlation between transfer functions for Rnd-E and Sin-E(CS, i.e., constant strain); the few points that disagree reflect difficulties in implementing the constant-strain test. The variation of the input voltage for sinusoidal excitation at constant and variable strain is presented in Fig. 7*b*; the input voltage for the Sin-E(CS) test shows a decrease towards resonance, where the transfer function is maximum.

From these results, one may hypothesize that the time superposition of different frequency components in Rnd-E leads to the equal shearing of energy losses across the imposed frequency bandwidth. Thus, testing with random excitation and a signal analyzer provides a linearized system response. While it is believed that computed parameters correspond to the optimized linear model of the system (Ewins 1984), they apply only to the imposed strain level.

Figure 8 shows velocity and damping data obtained at strains varying between $10^{-7} < \gamma < 10^{-4}$. Note that random noise excitation and the signal-processing procedures previously described permit testing to strains less than one order of magnitude smaller than the conventional sine-sweep procedure (the lowest strain reached in our laboratory was $\gamma \approx 10^{-8}$, which corresponds to a low level of mechanical background noise). Damping is almost constant at low shear strains; this indicates the presence of a non-hysteretic loss mechanism at low strain (Toksöz and Johnston 1981; Santamarina and Cascante 1996). Overall, and at this scale, velocity and damping from Rnd-E are in good agreement with the Sin-E results. Thus, the violation of assumptions made in signal processing does not seem to have a major effect on parameters computed at this strain level.

Multi-Mode Testing: Poisson's Ratio and Field Parameters

Poisson's ratio at low strain levels can be computed once Young's modulus (flexural mode; Eq 7) and shear modulus (torsional mode; Eq 8) are known:

$$\nu = \frac{1}{2}\frac{E}{G} - 1 \tag{15}$$

Hence, multi-mode velocity and damping data obtained with rod specimens can be used to compute the velocity and damping of plane P-waves in the field (Fratta and Santamarina 1996).

The flexural resonant frequency of a cantilever beam is an accurate method of determining Young's modulus E (see Kolsky 1963 for dispersion effects). The longitudinal wave velocity $V_L = (E/\rho)^{1/2}$ corresponds to constant compression, with $\lambda >> R$. However, the strain field induced in a rod by flexural excitation has a linear Navier variation of strain in the cross section, from tension to compression. In addition, the maximum strain in a cantilever beam in flexion also varies along the longitudinal axis. In analogy to the torsional mode, the volume-averaged strain is considered representative ϵ_{avg},

$$\epsilon_{avg} = \frac{2}{3\pi}\epsilon_{max} \tag{16}$$

where ϵ_{max} is the maximum axial strain at the base of the specimen.

Poisson's ratio was computed for a specimen subjected to incremental confinement by exciting the first flexural and torsional

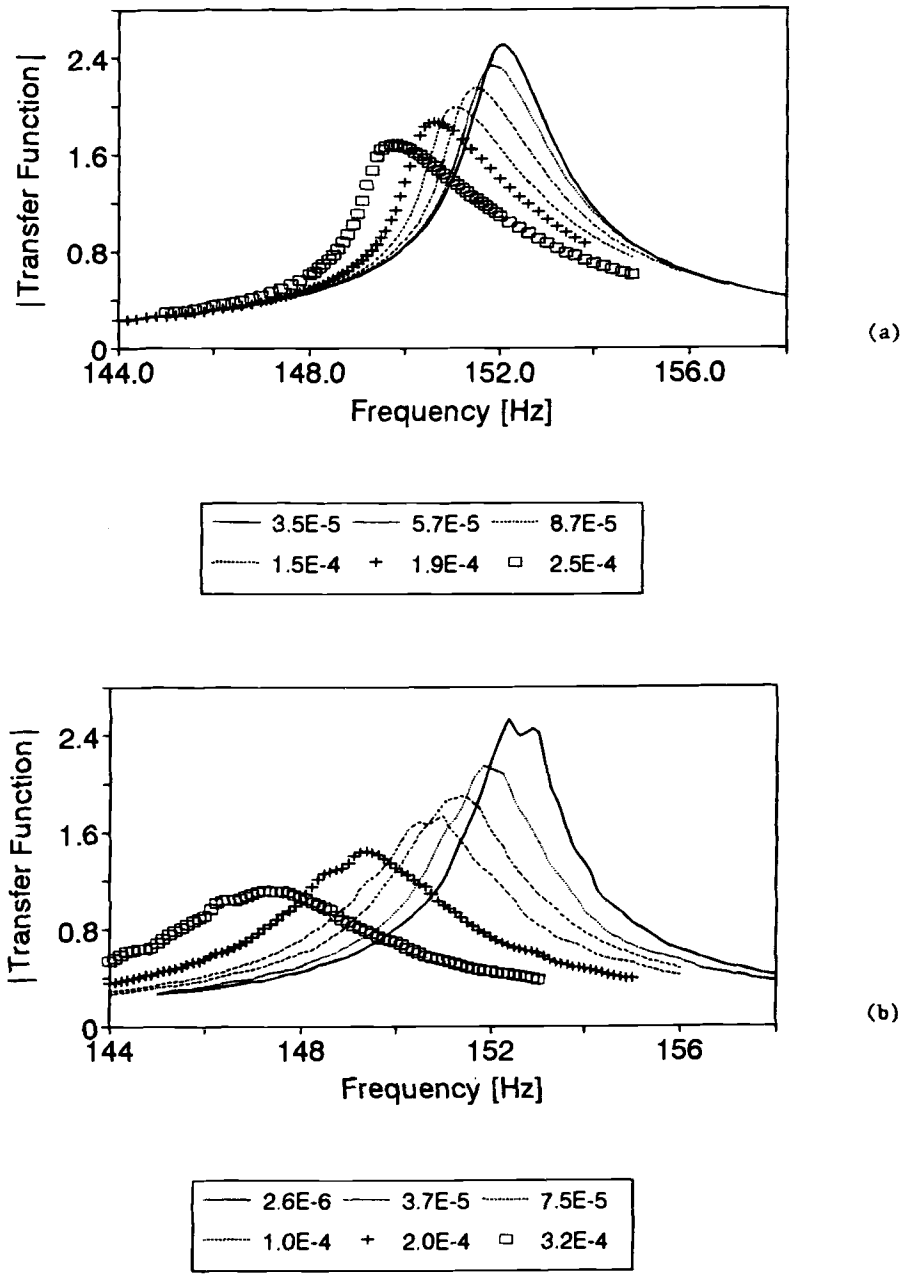

FIG. 6—*Evolution of the transfer function for different maximum shear strains:* (a) *sinusoidal excitation at constant input voltage; strain level computed with Eq 13;* (b) *random-noise excitation; strain level computed with Eq 14.*

modes at the same volumetric average strain levels (Fig. 9). Computed values are small, $\nu < 0.07$, and increase with pressure. This is in agreement with analytical predictions for regular and random packings (Petrakis and Dobry 1987; Chang 1990; Santamarina and Cascante 1996; Wang and Nur 1992).

Conclusions

Several issues in resonant column testing were experimentally or theoretically assessed. A closed-form solution was derived for flexural modes in a cantilever beam with an attached mass at the free end. It was shown that for the levels of confinement relevant to shallow geotechnical applications, the torsional frequency is about 60% higher than the flexural frequency. Mode coupling becomes important when the mass polar moment of inertia of the driving system is small in comparison with the mass polar moment of inertia of the sand specimen.

The error in low-strain stiffness obtained from torsional testing of solid specimens (non-annular) is less than 1% when the strain level at the periphery is below 1% of the reference strain.

Resonant column testing using narrow-band random noise excitation with averaging is a fast and accurate technique to determine low-strain wave propagation velocity and attenuation. The representative strain level for random noise excitations is calculated from the area under the output power spectral density. Measured parameters agree with results obtained with standard sinusoidal excitation.

As the strain level increases, the behavior of particulate materials becomes non-linear. The response obtained with sine-sweep excitation at constant input voltage shows a steep rise in the amplification curve on the low-frequency side. However, if the cause of non-

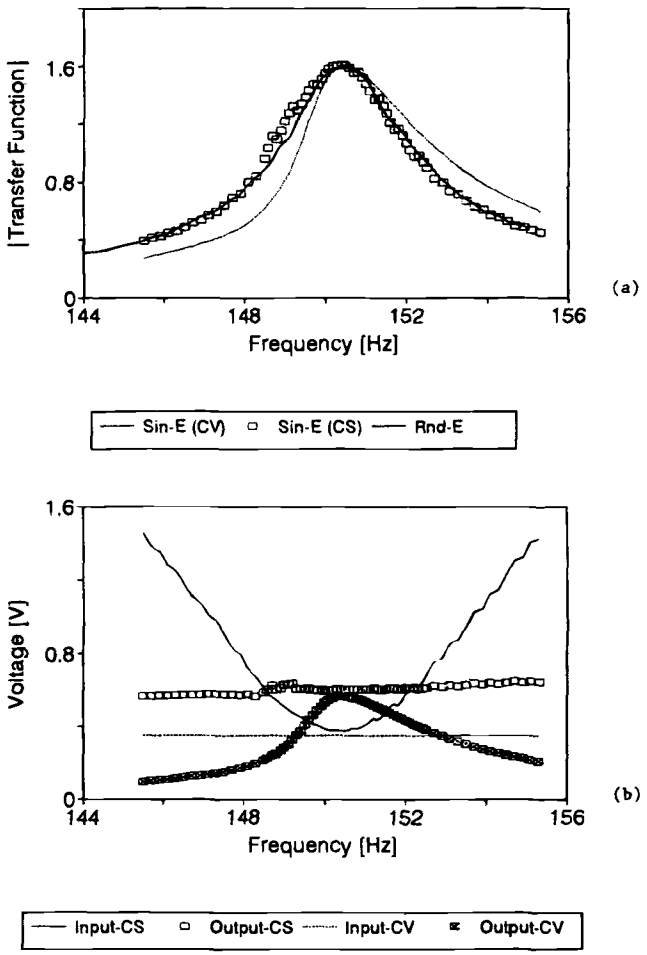

FIG. 7—*Type of excitation and non-linear response:* (a) *comparison of transfer functions: sinusoidal excitation at constant input voltage Sin-E(CV), sinusoidal excitation at constant strain Sin-E(CS)* ($\gamma = 10^{-3.6}$), *and random noise excitation (Rnd-E);* (b) *variation of input and output voltage for sinusoidal excitation at constant strain Sin-E(CS) and at constant input voltage Sin-E(CV).*

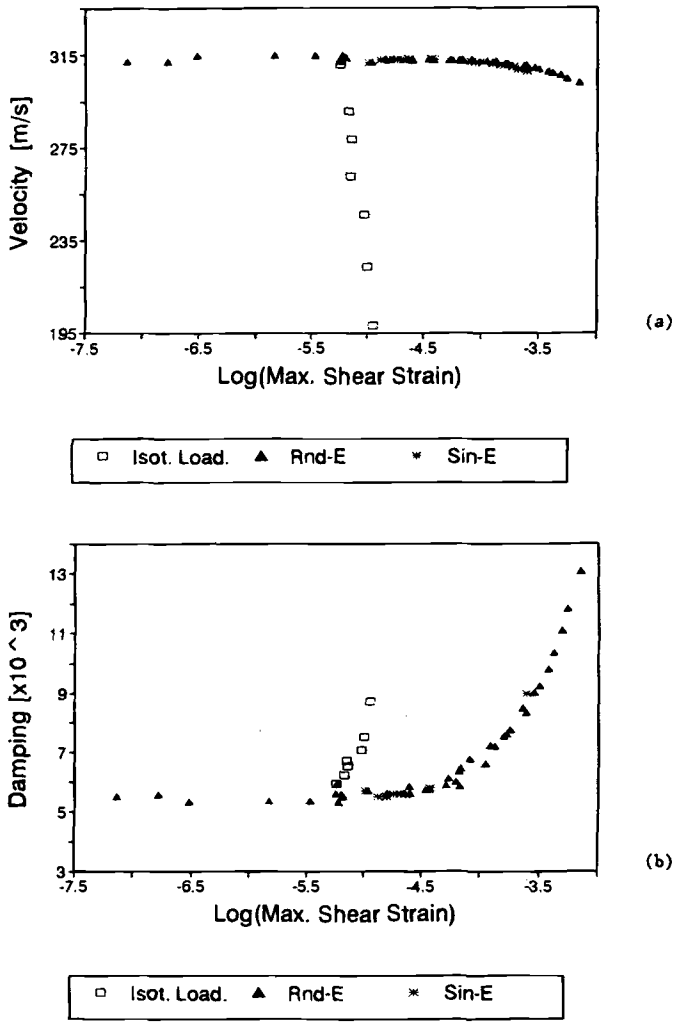

FIG. 8—*Velocity and damping at different strain levels for quartz sand isotropically loaded to 200 kPa and tested with random noise Rnd-E and sinusoidal Sin-E excitations:* (a) *shear wave velocity versus maximum shear strain;* (b) *damping versus maximum shear strain.*

linearity is amplitude dependent, then a sine-sweep test keeping the strain level constant renders a linearized system response for that strain level.

Random noise excitation also leads to a linearized system response for the imposed strain level, properly manifesting higher damping and lower frequency at the peak. A disadvantage of this result is that the linear response obtained with random noise and a signal analyzer may hide non-linear behavior.

Young's modulus and flexural damping can also be obtained from resonant-column testing by identifying the flexural mode. Multi-mode testing permits computing low-strain Poisson's ratio and field propagation parameters.

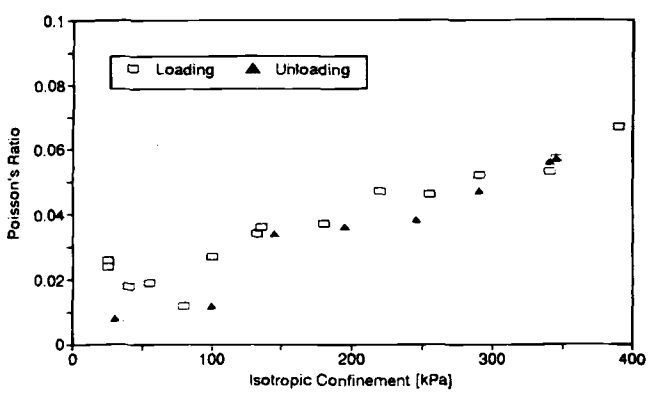

FIG. 9—*Low strain Poisson's ratio computed from the flexural and torsional modes—effect of confinement.*

Acknowledgments

This research is part of a study on wave-geomedia interaction and applications. Support was provided by the Natural Science and Engineering Research Council of Canada (NSERC) and the University of Waterloo ID-Program. The authors are indebted to Dr. Yassir for thoughtful comments and suggestions.

References

Achenbach, J. D., 1975, *Wave Propagation in Elastic Solids*, North-Holland Publishing Company, Amsterdam.

Aggour, M. S., Tawfiq, K. S., and Taha, M. R., 1988, "Impulse and Random Testing of Soils," *Proceedings*, Earthquake Engineering and Soil Dynamics II; Recent Advances in Ground-Motion Evaluation,

V. Thun and J. Lawrence, (Eds.), Geotechnical Special Publication No. 20, Park City, UT, pp. 346–358.

Amini, F., Tawfiq, K. S., and Aggour, M. S., 1988, "Cohesionless Soil Behavior Under Random Excitation," *Journal of Geotechnical Engineering Division, ASCE*, Vol. 114, No. 8, pp. 896–914.

Al-Sandad, H., Aggour, M. S., and Yang, J. C. S., 1983, "Dynamic Shear Modulus and Damping Ratio from Random Loading Test," *Geotechnical Testing Journal, ASTM*, Vol. 6, No. 3, pp. 120–127.

Ashmawy, A. K. and Drnevich, V. P., 1994, "A General Dynamic Model for the Resonant Column/Quasi-Static Torsional Shear Apparatus," *Geotechnical Testing Journal, ASTM*, Vol. 17, No. 3, pp. 337–348.

Avramidis, A. S. and Saxena, S. K., 1990, "The Modified 'Stiffened' Drnevich Resonant Column Apparatus," *Japanese Society of Soil Mechanics and Foundation Engineering*, Vol. 30, No. 3, pp. 53–68.

Bendat, J. S. and Piersol, A. G., 1993, *Engineering Applications of Correlation and Spectral Analysis*, 2nd ed., Wiley-Interscience, Inc., New York.

Bolton, M. D. and Wilson, J. M. R., 1990, "Soil Stiffness and Damping," *Structural Dynamics*, Kratzig et al., Eds., Balkema, Rotterdam, pp. 209–216.

Bourbie, T., Coussy, O., and Zinszner, B., 1987, *Acoustics of Porous Media*, Gulf Publishing Company, Houston, TX.

Cascante, G., 1996, "Low Strain Measurements with Mechanical Waves in Geomaterials—Implications in Geotomography," thesis submitted for the partial fulfillment of Ph.D. degree, University of Waterloo, Ontario.

Cascante, G. and Santamarina, J. C., 1996, "Interparticle Contact Behavior and Wave Propagation," *ASCE Geotechnical Journal*, Vol. 122, No. 10.

Chang, T., Misra, A., and Sundaram, S. S., 1990, "Micromechanical Modeling of Cemented Sands Under Low Amplitude Oscillations," *Geotechnique*, Vol. 40, No. 2, pp. 251–263.

Drnevich, V. P. and Richart, F. E. Jr., 1970, "Dynamic Prestraining of Dry Sand," *Journal of Soil Mechanics and Foundations Divisions, ASCE*, Vol. 96, No. SM2, pp. 453–469.

Drnevich, V. P., 1978, "Resonant-Column Problems and Solutions," *Dynamic Geotechnical Testing, ASTM STP 654*, pp. 384–398.

Drnevich, V. P., Hardin, B. O., and Shippy, D. J., 1978, "Modulus and Damping of Soils by the Resonant-Column Method," *Dynamic Geotechnical Testing, ASTM STP 654*, pp. 91–125.

Drnevich, V. P., 1985, "Recent Developments in Resonant Column Testing," *Proceedings*, Richart Commemorative Lectures, ASCE annual meeting, Detroit, MI, R. D. Woods, Ed., pp. 79–107.

EPRI, 1993, "Guidelines for Determining Design Basis Ground Motions," TR-102293, Research Project 3302, Electric Power Research Institute, Palo Alto, CA.

Ewins, D. J., 1984, *Modal Testing: Theory and Practice*, Research Studies Press LTD, England.

Fratta, D. and Santamarina, J. C., 1996, "Waveguide Device for Multi-Mode, Wideband Testing Wave Propagation in Soils," *ASTM Geotechnical Testing Journal*, Vol. 19, No. 2, pp. 130–140.

Hardin, B. O., 1965, "The Nature of Damping in Sands," *Journal of the Soil Mechanics and Foundations Division, ASCE*, Vol. 91, No. SM1, pp. 63–97.

Hardin, B. O. and Music, J., 1965, "Apparatus for Vibration of Soil Specimens During Triaxial Test," *Instruments and Apparatus for Soil and Rock Mechanics, ASTM STP 392*, American Society for Testing and Materials, West Conshohocken, PA, pp. 55–74.

Hardin, B. O. and Richart, F. E. Jr., 1963, "Elastic Wave Velocities in Granular Soils," *Journal of the Soil Mechanics and Foundations Division, ASCE*, Vol. 89, No. SM1, pp. 33–63.

Hardin, B. O. and Scott G. D., 1966, "Generalized Kelvin-Voigt Used in Soil Dynamics Study," *Journal of the Engineering Mechanics Division, ASCE*, February, pp. 143–156.

Isenhower, W. M., 1980, "Torsional Simple Shear/Resonant Column Properties of San Francisco Bay Mud," M.S. thesis, The University of Texas at Austin.

Ishihara, K., 1986, "Evaluation of Soil Properties for Use in Earthquake Response Analysis," *Geomechanical Modeling in Engineering Practice*, R. Dungar and J. A. Studer, Eds., Balkema, Rotterdam.

Kolsky, H., 1963, *Stress Waves in Solids*, Dover Publications, Inc., New York.

Petrakis, E. and Dobry, R., 1987, "Micromechanical Modeling of Granular Soil at Small Strain by Arrays of Elastic Spheres," Report CE-87-02, Department of Civil Engineering, Rensselaer Polytechnic Institute, Troy, NY.

Prange, B., 1981, "Resonant Column Testing of Railroad Ballast," *Proceedings*, Tenth International Conference on Soil Mechanics and Foundation Engineering, Stockholm, Vol. 3, pp. 273–278.

Richart, F. E. Jr., Hall, J. R., and Woods, R. D., 1970, *Vibration of Soils and Foundations*, Prentice Hall, Inc., Englewood Cliffs, NJ.

Roesset, J. M., 1991, "Energy Dissipation—State of the Art Report," EPRI NP-7337, Project 810-14, Vol. 1, Chap. 4, Electric Power Research Institute, Palo Alto, CA.

Santamarina, J. C. and Cascante, G., 1996, "Stress Anisotropy and Wave Propagation—A Micromechanical View," *Canadian Geotechnical Journal*, Vol. 33, October.

Stoll, Robert D., 1979, "Experimental Studies of Attenuation in Sediments (a)," *Acoustical Society of America*, Vol. 66, No. 4, October, pp. 1152–1160.

Toksöz, M. N. and Johnston, D. H., 1981, "Seismic Wave Attenuation," *Geophysics Reprint Series*, No. 2, Society of Exploration Geophysicists. Tulsa, OK.

Wang, Z. and Nur, A. 1992, "Elastic Wave Velocities in Porous Media: A Theoretical Recipe," *Seismic and Acoustic Velocities in Reservoir Rocks*, Vol. 2, SEG Geophysical Reprint Series, Tulsa, OK, pp. 1–35.

Ward, R. W. and Toksöz, M. N., 1971, "Causes of Regional Variation of Magnitude," *SSA Bulletin*, Vol. 61, pp. 649–670.

Wilson, S. D. and Dietrich, R. J., 1960, "Effect of Consolidation Pressure on Elastic and Strength Properties of Clay," *Proceedings*, ASCE Soil Mechanics and Foundations Division, Research Conference on Shear Strength of Cohesive Soils, Boulder, CO, ASCE, New York.

Woods, R. D., 1978, "Measurement of Dynamic Soil Properties," *Proceedings*, Specialty Conference on Earthquake Engineering and Soil Dynamics, Pasadena, CA ASCE, New York, Vol. 1, pp. 91–178.

Yu, P. and Richart, F. E., 1984, "Stress Ratio Effects on Shear Modulus of Dry Sands," *Journal of Geotechnical Engineering, ASCE*, Vol. 110, No. 3, pp. 331–345.